Transition probabilities of near-infrared Ce III lines from stellar spectra: applications to kilonovae

Nanae Domoto,[1] Jae-Joon Lee,[2] Masaomi Tanaka,[1,3] Ho-Gyu Lee,[2,4] Wako Aoki,[5,6] Miho N. Ishigaki,[5] Shinya Wanajo,[7,8] Daiji Kato,[9,10] and Kenta Hotokezaka[11,12]

[1]*Astronomical Institute, Tohoku University, Aoba, Sendai 980-8578, Japan*
[2]*Korea Astronomy and Space Science Institute, 776 Daedeok-daero, Yuseong-gu, Daejeon, 34055, Republic of Korea*
[3]*Division for the Establishment of Frontier Sciences, Organization for Advanced Studies, Tohoku University, Sendai 980-8577, Japan*
[4]*Space Policy Research Center, Science and Technology Policy Institute, 370 Sicheong-daero, Sejong, 30147, Republic of Korea*
[5]*National Astronomical Observatory, 2-21-1 Osawa, Mitaka, Tokyo 181-8588, Japan*
[6]*Astronomical Science Program, The Graduate University for Advanced Studies, SOKENDAI, 2-21-1 Osawa, Mitaka, Tokyo 181-8588, Japan*
[7]*Max-Planck-Institut für Gravitationsphysik (Albert-Einstein-Institut), Am Mühlenberg 1, D-14476 Potsdam-Golm, Germany*
[8]*Interdisciplinary Theoretical and Mathematical Sciences Program (iTHEMS), RIKEN, Wako, Saitama 351-0198, Japan*
[9]*National Institute for Fusion Science, 322-6 Oroshi-cho, Toki 509-5292, Japan*
[10]*Interdisciplinary Graduate School of Engineering Sciences, Kyushu University, Kasuga, Fukuoka 816-8580, Japan*
[11]*Research Center for the Early Universe, Graduate School of Science, University of Tokyo, Bunkyo, Tokyo 113-0033, Japan*
[12]*Kavli IPMU (WPI), UTIAS, The University of Tokyo, Kashiwa, Chiba 277-8583, Japan*

ABSTRACT

Kilonova spectra provide us with information of r-process nucleosynthesis in neutron star mergers. However, it is still challenging to identify individual elements in the spectra mainly due to lack of experimentally accurate atomic data for heavy elements in the near-infrared wavelengths. Recently, Domoto et al. (2022) proposed the absorption features around 14500 Å in the observed spectra of GW170817/AT2017gfo as Ce III lines. But they used theoretical transition probabilities (gf-values) whose accuracy is uncertain. In this paper, we derive the astrophysical gf-values of the three Ce III lines, aiming at verification of this identification. We model high resolution H-band spectra of four F-type supergiants showing the clear Ce III absorption features by assuming stellar parameters derived from optical spectra in literatures. We also test the validity of the derived astrophysical gf-values by estimating Ce III abundances in Ap stars. We find that the derived astrophysical gf-values of the Ce III lines are systematically lower by about 0.25 dex than those used in previous work of kilonovae, while they are still compatible within the uncertainty range. By performing radiative transfer simulations of kilonovae with the derived gf-values, we find that the identification of Ce III as a source of the absorption features in the observed kilonova spectra still stands, even considering the uncertainties in the astrophysical gf-values. This supports identification of Ce in the spectra of GW170817/AT2017gfo.

Keywords: line: identification — stars: neutron — stars: general — atomic data

1. INTRODUCTION

Binary neutron star (NS) mergers have been considered as promising sites of r-process nucleosynthesis (e.g., Eichler et al. 1989; Freiburghaus et al. 1999; Goriely et al. 2011; Korobkin et al. 2012; Wanajo et al. 2014). In 2017, associated with the detection

Corresponding author: Nanae Domoto
n.domoto@astr.tohoku.ac.jp

of gravitational waves (GWs) from a NS merger (GW170817, Abbott et al. 2017a), the electromagnetic counterpart AT2017gfo was observed (Abbott et al. 2017b). The observed properties of AT2017gfo in ultraviolet, optical, and near-infrared (NIR) wavelengths are consistent with the theoretical expectation of a kilonova (Li & Paczyński 1998; Metzger et al. 2010), thermal emission from NS merger ejecta powered by radioactive decays of r-process nuclei (e.g., Arcavi et al. 2017; Evans et al. 2017; Pian et al. 2017; Smartt et al. 2017; Utsumi et al. 2017; Valenti et al.

2017). This electromagnetic counterpart has provided us with evidence that NS mergers are sites of r-process nucleosynthesis (e.g., Kasen et al. 2017; Perego et al. 2017; Shibata et al. 2017; Tanaka et al. 2017; Kawaguchi et al. 2018; Rosswog et al. 2018).

To extract the detailed information of elements synthesized in NS merger ejecta, it is important to identify the individual elements. However, element identification in the kilonova spectra remains challenging. This is mainly due to lack of atomic data for heavy elements. While detailed spectral studies require spectroscopically accurate atomic data, such data for heavy elements have been highly incomplete, especially for the NIR wavelengths. So far, the absorption features around 8000 Å in the photospheric spectra of AT2017gfo have been identified as Sr II (Watson et al. 2019; Domoto et al. 2021; Gillanders et al. 2022), although the same features may be caused by He I (Perego et al. 2017; Tarumi et al. 2023).

Recently, Domoto et al. (2022) systematically studied kilonova spectra over the entire wavelength range. They identified important elements that produce strong transitions in kilonvoae, such as Ca, Sr, Y, Zr, Ba, La, and Ce. Then, they constructed a hybrid line list combined with experimentally accurate data for important elements and complete theoretical data for weak transitions of the other elements (Tanaka et al. 2020). By performing radiative transfer simulations, they found that the broad line features at ∼13000 Å and 14500 Å in the spectra of AT2017gfo can be explained by La III and Ce III, respectively. However, this identification can be still a subject of discussion as they adopted the transition probabilities (i.e., gf-values) of the La III and Ce III lines from theoretical calculations (Tanaka et al. 2020) due to lack of experimental measurements.

The lack of experimental atomic data is problematic in any spectra for astrophysical objects, such as stars. Compared with the optical region, line identification in stellar spectra in the NIR region is incomplete and still in progress (e.g., Matsunaga et al. 2020). Also, as few experiments have been performed on heavy elements such as lanthanides, gf-values from theoretical calculations are commonly used even for the optical wavelengths. In many cases, no or few data are provided for the NIR wavelengths (e.g., Biémont et al. 1999; Quinet & Palmeri 2020).

In general, the accuracy of atomic calculations is difficult to assess without experimental measurements. It has been shown that the theoretical gf-values for given ions differ from the experimental values several times for strong transitions, and even more for weak transitions (see, e.g., Appendix of Domoto et al. 2022). The

gf-values directly affect the absorption depths in the spectra, which influences derived parameters, e.g., abundances. In the case of kilonova model of Domoto et al. (2022), the absorption features at the NIR wavelengths can disappear if the gf-values of the NIR lines are ∼ 10 times smaller than the values they adopted. Therefore, it is important to measure the gf-values to firmly identify elements in kilonova spectra.

For the use in astrophysics, one can estimate the gf-values of atomic lines by using stellar spectra. This is often called as "astrophysical gf-values". Such work has been performed for many metal lines in the NIR wavelengths using the spectra of well-observed stars, e.g., the Sun (e.g., Meléndez & Barbuy 1999). In fact, it has been shown that the astrophysical gf-values can be useful to extract elemental information from stars without laboratory experiments (Hasselquist et al. 2016; Cunha et al. 2017).

In this paper, we derive the astrophysical gf-values of three Ce III lines at the H-band (around 1.6 μm) using high resolution stellar spectra. This aims to verify the identification of Ce in the spectra of AT2017gfo. Note that we cannot test the absorption by La III in the same way, because the La III lines at rest lie in the wavelength region of strong atmospheric absorption. In Section 2, we describe the targeted Ce III lines in more detail. We present the stellar spectra showing the Ce III line features in Section 3, and derive the gf-values of the Ce III lines by modeling these spectra in Section 4. In Section 5, we apply the derived gf-values of the Ce III lines to kilonova spectra by performing radiative transfer simulations. Finally, we give a summary in Section 6. We also show the validity of our results by estimating the Ce abundances with Ce III lines in Ap stars in Appendix A. Throughout of the paper, line wavelengths are written as those in vacuum unless otherwise mentioned.

2. CE III LINES AT H-BAND

We focus on the three Ce III lines at the H-band (Table 1). It has been shown that these are the strongest lines of Ce III in the NIR region, which can produce broad absorption features in kilonova spectra (Domoto et al. 2022). In fact, these lines have been detected in the spectra of Ap/Bp stars that exhibit enhanced Ce abundances (Hubrig et al. 2012; Chojnowski et al. 2019; Tanaka et al. 2023).

Although the transition wavelengths of these lines have been measured by experiments (Johansson & Litzén 1972), their transition probabilities are experimentally unknown. Thus, Domoto et al.

Table 1. The targeted Ce III lines at H-band.

λ_{vac}[a] ($\text{\AA}$)	λ_{air}[b] ($\text{\AA}$)	E_{lower}[c] (cm^{-1})	E_{upper}[d] (cm^{-1})	Theoretical $\log gf$[e]				Astrophysical $\log gf$[f]			
				(1)	(2)	(3)	(4)	(5)	(6)	(7)	This work
15851.880	15847.550	1528.32	7836.72	−0.613	−0.838	−1.030	−1.190	−0.439	−0.673	−2.105	−0.861
15961.157	15956.797	0.00	6265.21	−0.721	−0.926	−1.120	−1.290	−2.926	−1.098	−0.345	−0.966
16133.170	16128.763	3127.10	9325.51	−0.509	−0.722	−0.920	−1.070	−0.429	−1.950	−0.920	−0.702

Note— [a] Vacuum transition wavelength.

[b] Air transition wavelength.

[c] Lower energy level.

[d] Upper energy level.

[e] gf-values from theoretical calculations (1: Tanaka et al. 2020, see also Domoto et al. 2022; 2: Wyart & Palmeri 1998; 3: taken from Hubrig et al. 2012 and Chojnowski et al. 2019. These values were computed in the same way as in Biémont et al. 2002 and provided to Hubrig et al. 2012 and Chojnowski et al. 2019 as private communication; 4: Carvajal Gallego et al. 2021). For (1) and (4), theoretical gf-values are shown as they are, without calibration by considering the differences in the theoretical energy levels relative to the experimental energy levels.

[f] Astrophysical gf-values in the APOGEE line list (5: Table 7 of Shetrone et al. 2015; 6: taken from here through the SDSS Science Archival Server (SAS), see Holtzman et al. 2018; 7: taken from here through the SDSS SAS, see Smith et al. 2021), and those derived in this work (Section 4).

(2022) adopted the theoretical results of Tanaka et al. (2020). Other theoretical calculations are also available, i.e., used for studies of optical stellar spectra (Wyart & Palmeri 1998; Biémont et al. 2002) and for application to kilonovae (Carvajal Gallego et al. 2021). However, it is usually difficult to assess the accuracy of these calculations, and the gf-values vary over the range of ~ 0.5 dex as shown in Table 1.

Recently, the APOGEE survey has observed many Galactic stars at the H-band with the spectral resolution of $R \sim 22500$ (Majewski et al. 2017). To analyze the APOGEE spectra, the line lists for the H-band have been provided (Shetrone et al. 2015; Holtzman et al. 2018; Smith et al. 2021). They collected the atomic data from theoretical and experimental studies, and adjusted the gf-values by fitting those to the spectra of the Sun and Arcturus. It is shown that such astrophysical gf-values can improve the agreement between the observed spectra and the model spectra. In fact, the APOGEE line lists include the three Ce III lines that we focus on (Table 1). However, their astrophysical gf-values are quite uncertain, because there is no clear Ce III absorption in the spectra of the Sun and Arcturus. As a result, the gf-values vary by an order of magnitude across the different versions of the APOGEE line lists. This fact demonstrates that, if lines are not clearly detected in the spectra which is the case of Ce III lines for the Sun and Arcturus, it is difficult to derive the astrophysical gf-values even though the spectra are well characterized. To derive gf-values of the Ce III lines, we select stars clearly showing these Ce III line features (Section

3), although the uncertainties in stellar parameters can be larger than those of well-known stars such as the Sun and Arcturus (Section 4.3).

We mention that near the three lines, there is another Ce III line at 15964.93 $\text{\AA}$. According to the theoretical gf-values of this line (−1.272 by Tanaka et al. 2020, −1.660 by Biemont et al., see Chojnowski et al. 2019, or −1.690 by Carvajal Gallego et al. 2021), this line is weaker than the three Ce III lines. In fact, it is found that the absorption at this wavelength is usually dominated by the strong Si I $\lambda 15964.41$ $\text{\AA}$ line (see Figure 1). Thus, we will not focus on this line in this work.

3. STELLAR SPECTRA WITH CE III LINES

3.1. *Sample selection*

Compared with the NIR wavelengths, the line list in the optical region is more comprehensive and accurate. Ce abundances in many stars are indeed reported from optical observations, e.g., in Hypatia Catalog for Solar neighborhoods (Hinkel et al. 2014), the catalogue of luminous stars (Luck 2014), and the catalogue of chemically peculiar (CP) stars (Ghazaryan et al. 2018). While not all the stars in these catalogues have Ce abundances, measurements are available for a good fraction of stars. Thus, we will derive the astrophysical gf-values of the Ce III lines using the stars that (1) show the Ce III line features in the NIR H-band and (2) have known Ce abundances from optical spectra.

We obtain NIR H-band high resolution spectra from the spectral archive of the Immersion GRating INfrared Spectrometer (IGRINS, Park et al. 2014; Mace et al.
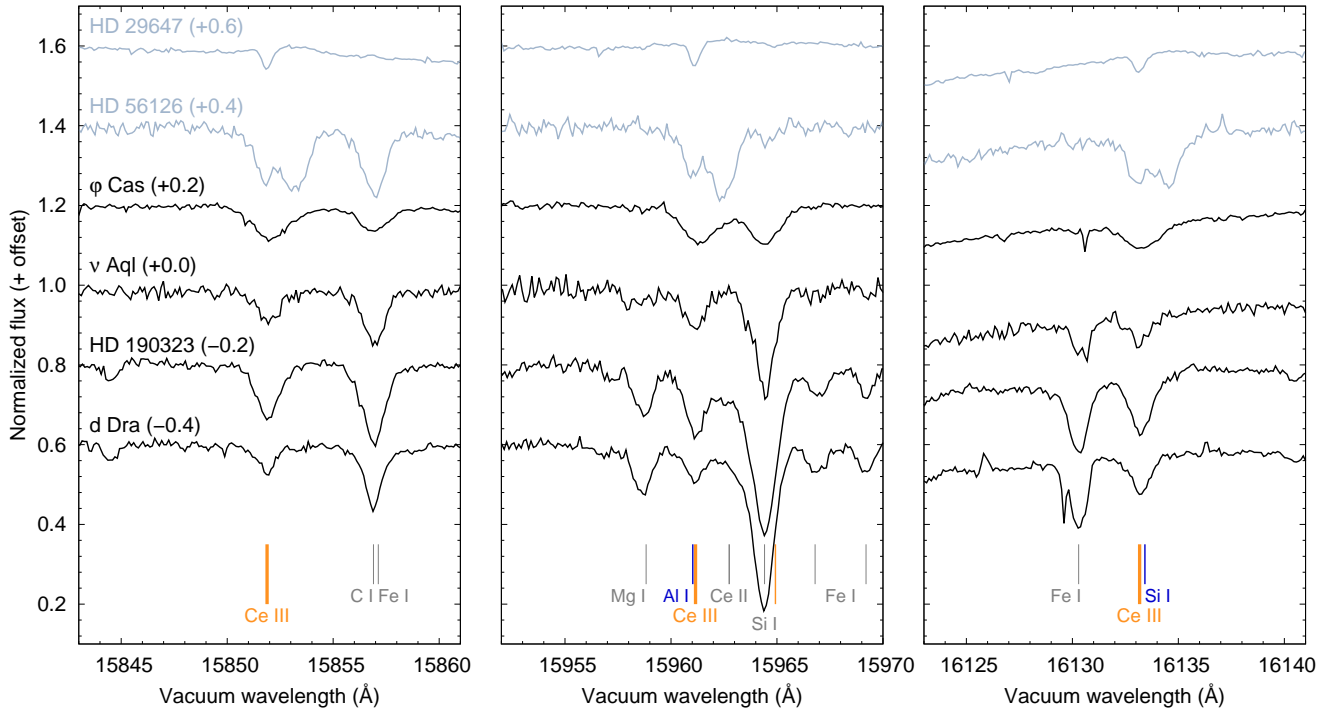
Figure 1. The IGRINS spectra around the Ce III lines of the selected stars. Black and gray lines show the spectra for the objects used as the final sample and for the excluded objects, respectively (see the text). The positions of the three Ce III lines that we focus on are indicated by thick orange lines (Table 1), while that of another Ce III line is also indicated by thin orange line (see Section 2). Al I and Si I lines that may contaminate the Ce III lines are labeled in blue. Other lines are also shown in gray.

2016, 2018). IGRINS provides spectra spanning the full H and K bands with the spectral resolution of $R \sim 45000$. The Raw & Reduced IGRINS Spectral Archive (RRISA)[1] contains the IGRINS archive for the period of July 2014–December 2021 on the 2.7 m Harlan J. Smith Telescope at McDonald Observatory, the Discovery Channel Telescope at Lowell Observatory, and the Gemini south telescope. RRISA includes IGRINS data from more than 850 nights on-sky, resulting in 2800 unique target observations from over 3000 hours of the total science time. RRISA also includes the IGRINS observations of > 1200 distinct A0V standard stars.

RRISA provides reduced one-dimensional (1D) spectra processed using the IGRINS pipeline (Lee et al. 2017). The pipeline applies flat-fielding and flagging of bad pixels, and the 1D spectra are extracted using the optimal extraction of Horne (1986). The wavelength solutions are derived using OH lines from sky spectra. In the H-band, the accuracy of wavelength solution is bet-

ter than 0.01 Å (~ 0.2 km s^{-1}). RRISA further refines the wavelength of the pipeline product by improving the pixel alignment between the A0V star spectrum and the target spectrum using strong telluric sky lines between 16452–16458 Å and 21740–21752 Å in the H- and K-band, respectively. Telluric absorption is corrected using the spectra of A0V stars observed closely in time and airmass with intrinsic features of A0V stars removed using a model spectrum of the Vega (Castelli & Kurucz 1994).

We crossmatch the RRISA archive with the two stellar catalogues of measured abundances: Luck (2014) and Ghazaryan et al. (2018). Not all entries in these catalogues have Ce abundances reported, and they are not used as we need abundance information to derive the gf-values (see below). Luck (2014) reports abundances for 451 luminous stars including Ce measurement for 448 stars. RRISA contains spectra for 27 of them. Ghazaryan et al. (2018) reports abundances of 429 CP stars with 121 stars of Ce measurement. RRISA contains spectra of 8 stars.
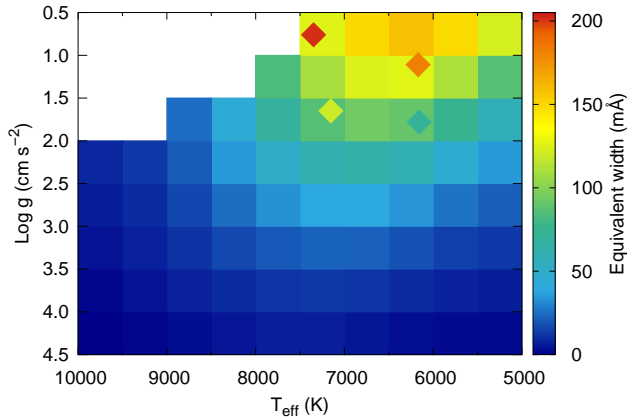
---

[1] https://igrinscontact.github.io/

Figure 2. EW of the Ce iii λ15961.157 Å line in the model spectra (colormap) and in the observed spectra (diamonds). Note that the region without color (upper left) is the parameter space where no ATLAS model exists.

For the matched data, we apply Doppler correction using strong C i, Si i, and Fe i lines. Then, we visually check the absorption lines at the wavelengths of the Ce iii lines. We impose the detection of all three lines to ensure the origin of these lines. As a result, six stars showing clear Ce iii line features are selected: HD 29647, HD 56126, φ Cas, ν Aql, HD 190323, and d Dra. The spectra of six stars around the regions of the Ce iii lines are shown in Figure 1.

While the six stars are selected above, we decide not to use two out of them: HD 29647 and HD 56126 (gray lines in Figure 1). This is because their atmospheric parameters are found to be rather uncertain, although they are listed in the catalogues. For HD 29647, a HgMn star (Straizys et al. 1985), Adelman et al. (2001) have reported the atmospheric parameters, but they mentioned that the parameters are not very accurate. For HD 56126, a post-AGB star (e.g., Hony et al. 2003), atmospheric parameters seem to change depending on the epoch when spectra are taken (De Smedt et al. 2016; Puķītis et al. 2022). Puķītis et al. (2022) also pointed out the chemical depletion of neutron-capture elements in other post-AGB star, likely due to dust condensation. Also, the IGRINS spectrum of HD 56126 shows double-peak like features, whose origins are unknown.

Finally, we use four stars as our samples (black lines in Figure 1). The S/N ratios of the spectra around the targeted Ce iii lines are > 100 for ν Aql and > 200 for the others. Since the Ce iii λ15851.88 Å and λ16133.170 Å lines are located around the broad hydrogen features, the spectra are normalized by fitting the broad features as a pseudo-continuum. After the normalization, we measure the equivalent widths (EWs) of the Ce iii lines

by Gaussian fitting (see the top panels of Figure 3 as examples). The measured EWs of the Ce iii lines in each star are shown in Table 3, which are used to derive those astrophysical gf-values in Section 4.

3.2. *Properties of sample stars*

The four stars in our final sample are all F-type supergiants (see Table 2). Our primary catalogue of Luck (2014) consists primarily of (super)giants with $T_{\rm eff} \sim$ 4000–8000 K, and the Ce iii lines are only seen in warmer supergiants of $T_{\rm eff} > 6000$ K. To check the presence of the Ce iii lines in wider parameter range of $T_{\rm eff}$ and surface gravity log g, we also crossmatch the RRISA with Hinkel et al. (2014). RRISA contains spectra of 132 sources out of 2685 stars from Hinkel et al. (2014), primarily of nearby dwarf stars. But none of the spectra show clear signature of the Ce iii lines. We further check RRSIA with $T_{\rm eff}$ and log g from the PASTEL catalogue (Soubiran et al. 2016). RRISA contains spectra of 168 stars with $T_{\rm eff} \sim$ 5500–8000 K, mostly dwarfs with some (super)giants. Note that this catalogue does not provide abundance measurements and is not subject to our analysis of deriving the gf-values. We find five stars showing the Ce iii line features, which are the same four stars as our sample selected from Luck (2014) and an additional F-type supergiant.

We briefly discuss the reason why the Ce iii lines tend to appear in warm supergiants. To see the behavior of the Ce iii absorption in spectra, we generate model spectra for the wavelength regions around the Ce iii lines, varying $T_{\rm eff}$ and log g. We use Turbospectrum (Plez 2012) implemented through iSpec (Blanco-Cuaresma et al. 2014; Blanco-Cuaresma 2019) to perform spectral synthesis, assuming local thermodynamic equilibrium (LTE). The parameter ranges are $T_{\rm eff} = 5000$–10000 K and log $g = 0.5$–4.5 dex with intervals of 500 K and 0.5 dex, respectively. For simplicity, we fix the microturbulent velocity $\xi = 2$ km s^{-1}, the solar abundance ratio (Asplund et al. 2009), and the projected rotational velocity $v \sin i = 10$ km s^{-1} as typical values (e.g., Matsunaga et al. 2020), and assume the macroturbulent velocity $v_{\rm mac} = 0$ km s^{-1} (see also Section 4.1). We use ATLAS, 1D plane-parallel atmosphere model (Castelli & Kurucz 2003). For the atomic data, we use the APOGEE line list (Holtzman et al. 2018; Smith et al. 2021, see Section 4.1) as a baseline, with the line list of the Ce iii lines from Domoto et al. (2022). These choices do not affect the dependence on $T_{\rm eff}$ and log g discussed here.

Table 2. Adopted stellar parameters for the sample stars.

Star	Spectral type	Model	$T_{\rm eff}$ (K)	$\log g$ (cm s^{-2})	[Fe/H]	ξ (km s^{-1})	$v \sin i$ (km s^{-1})	[Al/H]	[Si/H]	[Ce/H]	$\sigma_{\rm [Ce/H]}{}^a$
φ Cas	F0Ia	ATLAS	7347	0.76	-0.07	5.21	23.0*	0.00^b	0.49	0.16	0.30
ν Aql	F2Ib	ATLAS	7152	1.65	0.10	3.74	12.0**	0.22	0.32	0.27	0.22
HD 190323	F8Ia	MARCS	6169	1.11	0.12	4.31	15.0‡	0.42	0.27	0.25	0.15
d Dra	F8Ib-2	MARCS	6157	1.78	-0.10	3.93	10.0†	0.16	0.06	0.27	0.24

Note— All the parameters are adopted from Luck (2014), but $v \sin i$ from Abt & Morrell (1995) (*), Uesugi & Fukuda (1970) (**), Lyubimkov et al. (2012) (†), and estimated in this work using the Ce III line because of no available measurement (‡).
^{a} Standard deviations of the Ce abundances measured in Luck (2014) (see Section 4.3).
^{b} The solar abundance (Asplund et al. 2009) is assumed because it is not measured in Luck (2014).

Since the dependence of the absorption on the atmospheric parameters is expected to be the same among the Ce III lines, we focus only on the Ce III $\lambda 15961.157$ Å line. Note that this Ce III line may be contaminated by Al I $\lambda 15961.03$ Å line at lower $T_{\rm eff}$ and higher $\log g$, although the Ce III line is dominant (Section 4.1). We measure the EWs of the Ce III line in the model spectra by Gaussian fitting as done in the observed spectra. The measured EWs for different $T_{\rm eff}$ and $\log g$ are shown in Figure 2. It is seen that the EW of the Ce III line peaks at $T_{\rm eff} \sim$ 6000–7000 K and $\log g < 2$. The peak $T_{\rm eff}$ can be understood as the region where the doubly ionized Ce is the most abundant under LTE. Also, the line becomes strong toward low gravity, due to low-density and geometrically thick atmosphere (Gray 2005). A similar trend is observed for other lines of metal ions (Matsunaga et al. 2020).

We also show the observed EWs of the Ce III $\lambda 15961.157$ Å line for the four sample stars as shown with diamonds in Figure 2. Although the Ce abundances are not exactly same as the solar abundances for these stars, it is seen that the observed trend is consistent with the trend in our model grid. Also, models are consistent with the fact that only warm (F-type) supergiants show the Ce III lines but not normal dwarfs.

Of course, the behavior of the Ce III lines are also dependent on the Ce abundance. If the Ce abundance is higher, the parameter range of $T_{\rm eff}$ and $\log g$ showing the Ce III lines becomes wider. For example, as shown in Figure 1, HD 29647 shows Ce III absorption in the NIR wavelengths even under high temperature and strong surface gravity ($T_{\rm eff} \sim$ 12500 K and $\log g \sim 4$, Adelman et al. 2001), because the Ce abundance is ~ 3 dex higher than the solar value (see also Appendix A). We note that CP stars are main sequences; supergiants used in our analysis do not show such anomaly in abundances of lanthanides.
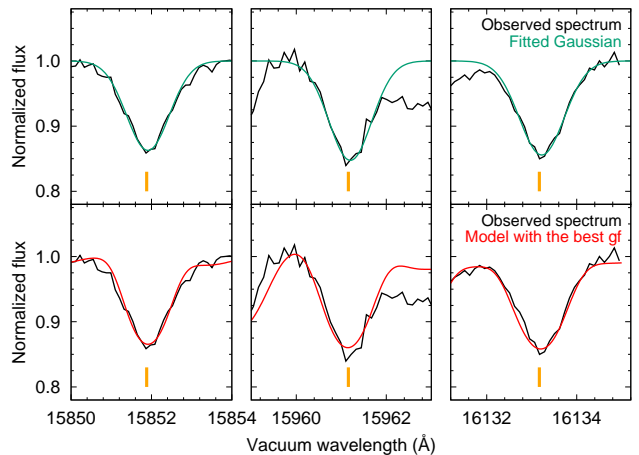

Figure 3. The Ce III lines of HD 190323 (black). In the top panels, the observed spectra are compared with the fitted Gaussian profile (green). In the bottom panels, the observed spectra are compared with the model spectra using the derived gf-values (red). Note that the observed spectrum at ~ 15963 Å of HD 190323 (the middle panels) may be affected by unknown lines.

4. ASTROPHYSICAL GF-VALUES OF THE CE III LINES

4.1. *Methods*

In this section, we derive the astrophysical gf-values of the Ce III lines. For each sample star, we perform spectral synthesis calculations with the fixed Ce abundances based on the measurements with the optical spectra, and then adjust gf-values. We use Turbospectrum (Plez 2012) through iSpec (Blanco-Cuaresma et al. 2014; Blanco-Cuaresma 2019) to synthesize spectra as in Section 3.2.

We adopt atmospheric parameters ($T_{\rm eff}$, $\log g$, metallicity, and ξ) derived from the analysis of optical spec-

tra. Luck (2014) provided the stellar parameters of sample stars using MARCS models (Gustafsson et al. 2008). For the stars with $T_{\rm eff}$ higher than ~ 6300 K, they also used ATLAS models (Castelli & Kurucz 2003). In our sample, when a star has two parameter sets determined using both models, we use the atmospheric parameters that better reproduce the H-band IGRINS spectra. Then, for spectral synthesis, we consistently use MARCS or ATLAS models used in the estimates of the adopted atmospheric parameters. The adopted atmospheric parameters and models of sample stars are summarized in Table 2.

We use the elemental abundances derived using the adopted atmospheric parameters in Luck (2014). Luck (2014) used observational data from multiple archives and provided abundances for each of the available data for a given star. When multiple abundance sets are provided for our sample stars, we simply take the averages. While all the elements are included in our calculations, only Ce, Al, and Si are important for our analysis: Ce abundances directly affect the absorption depths of the Ce III lines, while Al and Si may also affect the Ce III absorption due to the contamination by Al I $\lambda15961.03$ Å and Si I $\lambda16133.42$ Å lines, respectively. For the elements without measurements, we assume the solar abundances (Asplund et al. 2009). For example, the Al abundance for φ Cas is assumed as the solar abundance. But this assumption does not affect the results because most Al is expected to be ionized in a high $T_{\rm eff}$ (~ 7300 K) and low $\log g$ (~ 0.8 dex) atmosphere (see also Section 4.3 and Table 4). For all the samples, the contamination from the Al I and Si I lines for the Ce III absorption features are estimated to be $< 10\%$ and $< 30\%$, respectively, by measuring the EWs of the lines in the model spectra without the Ce III lines. The adopted abundances of important elements are also summarized in Table 2.

It should be cautioned that, although the Ce abundances are fixed in our analysis, they are also subject to the uncertainties (see also Section 4.3). The standard deviations of the Ce abundances measured in Luck (2014) are also shown in Table 2. We confirmed that the absorption of Ce II lines at the H-band (Cunha et al. 2017) is reasonably reproduced for HD 190323 and d Dra, which confirms the validity of the abundances. There is no or little Ce II absorption for φ Cas and ν Aql with $T_{\rm eff} > 7000$ K. Nevertheless, we emphasize that the Ce abundances in these two stars are rather robust, because they were derived using optical lines with experimental gf-values (Luck 2014).

Spectral synthesis also needs to consider effects of line broadening. It is usually difficult to separate the ef-

fects of $v \sin i$ and $v_{\rm mac}$ on the line profiles in F-type supergiants (e.g., Lyubimkov et al. 2012). Here, we ignore $v_{\rm mac}$ and consider only $v \sin i$. These parameters for φ Cas, ν Aql, and d Dra are taken from literatures (see Table 2). We find that these choices reasonably reproduce the line profiles in the IGRINS spectra. On the other hand, no measurement of $v \sin i$ for HD 190323 was found. Thus, we estimate $v \sin i$ using the Ce III lines in the IGRINS spectra (see Table 2). Although this is not very accurate measurement, this assumption does not affect our results.

The line list for other elements is also an important factor in the estimate of gf-values. This is because some Ce III lines are contaminated by Al I or Si I lines. Thus, the gf-values of these lines may affect the estimates of the gf-values of the Ce III lines. By comparing the H-band model spectra using the VALD (Piskunov et al. 1995; Kupka et al. 1999; Ryabchikova et al. 2015) and the APOGEE line lists (Holtzman et al. 2018; Smith et al. 2021), we find that the APOGEE line list reproduces the observed features of the IGRINS spectra better. Thus, we adopt the APOGEE line list for our analysis. Note that, as iSpec implements the APOGEE line list of DR13/14 (Holtzman et al. 2018), we updated the line list using the newest DR16 line list (Smith et al. 2021) except for hyperfine structure lines.

For the model spectra, we measure the EWs of the Ce III lines by Gaussian fitting as done in the observed spectra. These EWs are compared with those of the observed spectra (Section 3.1). Comparison is repeated by changing the gf-values of the Ce III lines. Finally, we adopt the gf-values that give the EWs in agreement with the EWs of the observed spectra. Examples of the final model spectra are shown in the bottom panels of Figure 3.

4.2. Results

The estimated gf-values of the three Ce III lines using the spectra of four stars are shown by blue dots in Figure 4, and listed in Table 3. As our final astrophysical gf-values of each Ce III line, we take the averages of those derived for each star. They are plotted as red dots in each panel of Figure 4, and listed in Table 1. The validity of our final gf-values is also discussed in Appendix A.

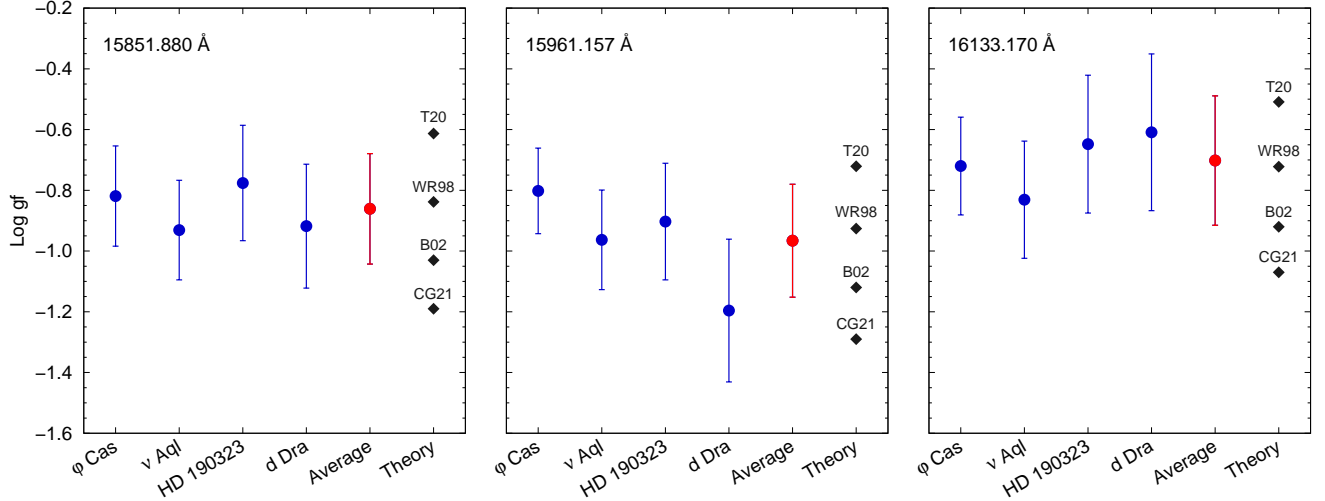The gf-values of the Ce III lines from available theoretical calculations are also shown by black diamonds

Figure 4. Astrophysical gf-values of the Ce III lines derived in four stellar spectra (blue dots), and their average (red dots). Each panel shows the results of each transition as shown in the legend. Black diamonds show the theoretical gf-values (T20: Tanaka et al. 2020; WR98: Wyart & Palmeri 1998; B02: Biemont et al., see Table 1; CG21: Carvajal Gallego et al. 2021). Error bars indicate the estimated systematic uncertainties (see Section 4.3 and Table 4).

Table 3. Observed EWs and derived gf-values for the three Ce III lines in four sample stars.

Star	EW (mÅ)	log gf	EW (mÅ)	log gf	EW (mÅ)	log gf
	15851.880 Å		15961.157 Å		16133.170 Å	
φ Cas	184	−0.82	201	−0.80	166	−0.72
ν Aql	102	−0.93	120	−0.96	96	−0.83
HD 190323	183	−0.78	182	−0.90	180	−0.65
d Dra	81	−0.92	71	−1.20	113	−0.61

in Figure 4 (see Table 1). All of our gf-values are consistently smaller than those of Tanaka et al. (2020), which were used for the kilonova model of Domoto et al. (2022). This suggests that the strength of absorption could have been overestimated in the kilonova model of Domoto et al. (2022) (see Section 5). On the other hand, it is seen that the estimated final gf-values are the closest to those of Wyart & Palmeri (1998), while higher than those of Biémont et al. (2002) and Carvajal Gallego et al. (2021). Overall, our gf-values of the Ce III lines, which are independently estimated from theoretical calculations, broadly agree with the available theoretical calculations within the margin of the estimated uncertainties discussed in Section 4.3.

4.3. Uncertainties in gf-values

Uncertainties in the astrophysical gf-values can be evaluated by considering the uncertainties in the stel-

lar parameters of each star. The systematic uncertainty of stellar parameters can generally be caused by difference in the analysis methods. Even with common atmospheric parameters and line lists, there remain variety in the abundances determined by different codes and methods (Hinkel et al. 2016) as well as different spectral data used in the analysis (Luck 2014). All of these factors can affect the depth of absorption lines, which leads to uncertainties in the astrophysical gf-values derived for the fixed Ce abundances.

We estimate the systematic uncertainties in our astrophysical gf-values by varying stellar parameters of each star. To take uncertainties of stellar parameters into account, we vary $T_{\rm eff}$ by ± 200 K, log g by ± 0.3 dex, [Fe/H] by ± 0.3 dex, and ξ by ± 0.5 km s^{-1}. Also, we vary [Al/H] and [Si/H] by ± 0.5 and ± 0.3 dex, respectively, which affect the level of the contamination. These ranges are typical systematic uncertainties caused

Table 4. Systematic uncertainties in the astrophysical gf-values of the Ce III lines for the fixed Ce abundances in each star.

Star	λ_{vac} (Å)	ΔT_{eff} (+200 K)	$\Delta \log g$ (+0.3 dex)	Δ[Fe/H] (+0.3 dex)	$\Delta \xi$ (+0.5 km s^{-1})	Δ[Al/H] (+0.5 dex)	Δ[Si/H] (+0.3 dex)	Δ_{sys}
φ Cas	15851.880	0.146	0.067	0.035	-0.018	-	-	0.165
	15961.157	0.105	0.085	0.029	-0.030	-0.002	-	0.141
	16133.170	0.139	0.070	0.034	-0.010	-	-0.022	0.161
ν Aql	15851.880	0.048	0.153	0.028	-0.017	-	-	0.164
	15961.157	0.054	0.151	0.025	-0.019	-0.015	-	0.164
	16133.170	0.067	0.151	0.046	-0.014	-	-0.088	0.193
HD 190323	15851.880	0.000	0.176	0.066	-0.030	-	-	0.190
	15961.157	0.003	0.179	0.057	-0.021	-0.031	-	0.192
	16133.170	0.018	0.175	0.100	-0.026	-	-0.099	0.227
d Dra	15851.880	-0.015	0.196	0.055	-0.011	-	-	0.204
	15961.157	-0.002	0.194	0.056	-0.005	-0.121	-	0.235
	16133.170	0.014	0.194	0.081	-0.014	-	-0.149	0.258

by different codes and methods used to determine stellar parameters (Hinkel et al. 2016). While Hinkel et al. (2016) used dwarfs to show these uncertainty ranges, the uncertainties for supergiants are similar to those in dwarfs (Luck 2014).

Table 4 summarizes the estimated systematic uncertainties in the astrophysical gf-values of the Ce III lines. Only the results for the positive shifts are shown, but the results for the negative shifts are smaller than the uncertainties given in Table 4 (see also Table 3 of Cunha et al. 2017). We find that the largest uncertainties are caused by T_{eff} or $\log g$. The systematic uncertainties in total in each gf-value for each star (Δ_{sys}) are estimated by taking root sum squares (Cunha et al. 2017). Note that the values of Δ_{sys} estimated here are the upper limits of the uncertainties: all the stellar parameters are not independent, and the uncertainties caused by each parameter may be cancelled among parameters (Cunha et al. 2017). In most cases, the total systematic uncertainties are smaller than 0.2 dex, and up to $\sim$ 0.26 dex. These systematic uncertainties are shown as the error bars for the blue dots in Figure 4.

Finally, we assign the systematic uncertainties of the average astrophysical gf-values by taking root mean squares of the Δ_{sys} in four stars. The systematic uncertainties in the gf-values for $\lambda 15851.880$ Å, $\lambda 15961.157$ Å, and $\lambda 16133.170$ Å lines are 0.182, 0.186, and 0.213, respectively (shown as the error bars for the red dots in Figure 4). It is worth noting that our astrophysical gf-values are broadly agree with available theoretical calculations, considering the systematic uncertainties.

Here we did not show the uncertainties in continuum levels of the observed spectra in Δ_{sys}. They may affect the observed EWs and in turn astrophysical gf-values. However, the uncertainties in continuum levels and their contributions to Δ_{sys} are estimated to be $\lesssim$ 1%, which are smaller than the uncertainties from most stellar parameters (see also Table 3 of Cunha et al. 2017).

Note that, although we fix the Ce abundances of each star to derive astrophysical gf-values, the Ce abundances are still uncertain within the range of $\lesssim$ 0.3 dex (standard deviations, Section 4.1). The Ce abundances scale the resultant gf-values: for example, if the Ce abundance is altered by the standard deviation (Table 2) to the positive direction, the derived gf-values are also affected by the same degree to the negative direction. Furthermore, it should be noted that the Ce abundances in Luck (2014) as well as the astrophysical gf-values here were derived under the assumption of LTE. Non-LTE treatment may affect the abundances of heavy elements (e.g., Mashonkina et al. 2005), especially in supergiants. This may result in systematic changes in the derived gf-values. Nevertheless, the fact that the derived gf-values are consistent among samples suggests that the Ce abundance of each star adopted in this work is reasonable. Independent measurements of stellar parameters may be able to reduce the uncertainties in the astrophysical gf-values, but this is beyond the scope of this work. The uncertainties present here are found not to significantly affect the final results on kilonova spectra, as discussed in Section 5.
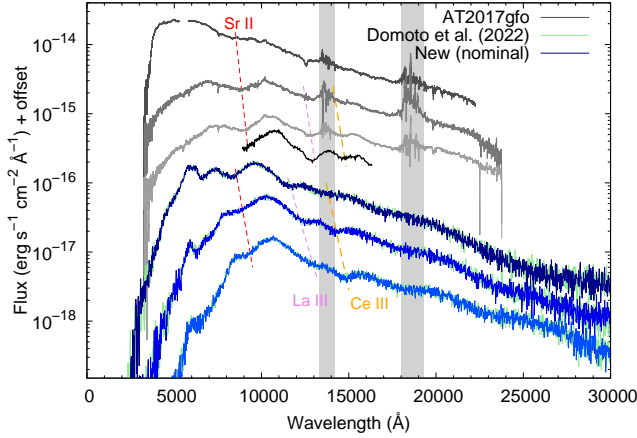
Figure 5. Comparison between the synthetic spectra (blue) and the observed spectra of AT2017gfo taken with the VLT (gray, Pian et al. 2017; Smartt et al. 2017) at $t = 1.5$, 2.5, and 3.5 days after the merger (dark to light colors). The spectrum taken with the HST at $t = 4.5$ days after the merger (Tanvir et al. 2017) is also shown in black line. The green curves are the synthetic spectra of Domoto et al. (2022, see their Figure 8). Spectra are vertically shifted for visualization. Gray shade shows the regions of strong atmospheric absorption.
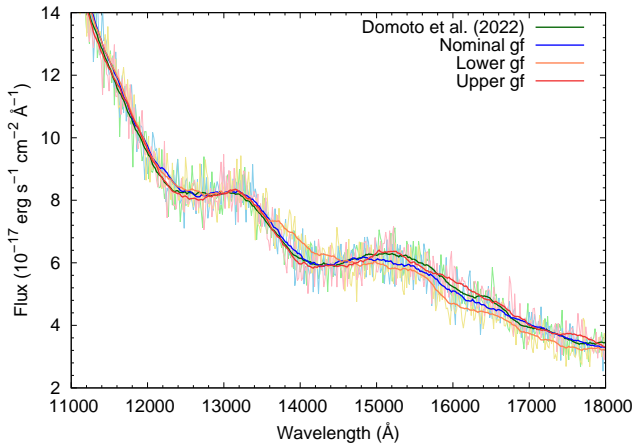
Figure 6. Enlarged view of the synthetic spectra for the NIR region at $t = 2.5$ days. Blue curves show the synthetic spectra using the derived gf-values, and green curves show those of Domoto et al. (2022). Orange and red curves show the synthetic spectra when using the lower and upper gf-values, which are considering the sum of the uncertainties negatively and positively, respectively (see the text). The curves in light colors show the original results, while those in dark colors show smoothed spectra for visualization.

5. APPLICATIONS TO KILONOVA SPECTRA

We apply the derived gf-values of the Ce III lines to calculate kilonova spectra. To calculate synthetic spectra of kilonovae, we use a wavelength-dependent ra-

diative transfer simulation code (Tanaka & Hotokezaka 2013; Tanaka et al. 2014, 2017, 2018; Kawaguchi et al. 2018, 2020). The photon transfer is calculated by the Monte Carlo method. The setup of simulation is identical to that in Domoto et al. (2022), but we adopt the final astrophysical gf-values of the three Ce III lines derived in Section 4. For more details of the simulation, we refer the readers to Domoto et al. (2022).

Figure 5 shows the comparison between our new synthetic spectra (blue) and the observed spectra of AT2017gfo taken with the Very Large Telescope (VLT) (gray) at $t = 1.5$, 2.5, and 3.5 days after the merger (Pian et al. 2017; Smartt et al. 2017). The observed spectra at $t = 4.5$ days after the merger taken with the Hubble Space Telescope (HST), which are not affected by telluric absorption, is also shown by a black line (Tanvir et al. 2017). We find that the absorption features around 14500 Å are caused by the Ce III lines in the new spectra. These features are blueshifted according to the velocity of the line-forming region at the NIR wavelengths, e.g., $v \sim 0.1\,c$ at $t = 2.5$ days. In fact, the features caused by the Ce III lines in the new synthetic spectra are almost the same as those in Domoto et al. (2022, green), which used the gf-values of Tanaka et al. (2020) (see Figure 6 for the enlarged view at $t = 2.5$ days). This is consistent with the observed features in the spectra of AT2017gfo.

To see the effects of the uncertainties in the gf-values to the spectra, we also perform the same simulations by varying the gf-values of the Ce III lines. Orange and red curves in Figure 6 show the results when using the lower and upper gf-values, respectively. Here, for the lower (upper) values, we take the averages of the estimated gf-values for each star negatively (positively) shifed by $\sigma_{[\mathrm{Ce/H}]}$, and then further shift the averages by Δ_{sys} negatively (positively). We find that the changes in fluxes around 14500 Å are $\sim 10\%$. The absorption features by Ce III are still seen even using the lower gf-values (orange curves), although the depth of absorption is weakened.

When using the final astrophysical gf-values, the Sobolev optical depths of the Ce III lines for the line forming region ($\rho \sim 10^{-14}$ g cm^{-3} and $T \sim 5000$ K, see Domoto et al. 2022) are ~ 4. The lower gf-values of the Ce III lines are smaller than the nominal values by a factor of ~ 2.7. Thus, even by adopting the lower gf-values, the Sobolev optical depths of the Ce III lines are still larger 1. This confirms the identification of Ce in the spectra of AT2017gfo.

The changes in gf-values of the strong lines affect not only absorption but also emission in the spectra. A stronger absorption tends to cause a stronger emis-

sion in P-Cygni type line profile. As shown in Figure 6, the increase of the gf-values results in the increase of the flux at emission component around the rest wavelengths, and vice versa. Note that, for particularly large gf-values (red and green lines), the optical depths of the Ce III lines are large enough that the depth of the absorption is saturated, while the effect in the emission component is still apparent.

6. SUMMARY

We have derived the astrophysical gf-values of the three Ce III lines at the H-band using the IGRINS spectra of four F-type supergiants. The derived gf-values are systematically lower by about 0.25 dex than those used in Domoto et al. (2022), but they are broadly agree with available theoretical calculations within the estimated uncertainties. Using the derived astrophysical gf-values of the Ce III lines, we have performed radiative transfer simulations of kilonovae. We have found that the Ce III lines with the new gf-values produce the absorption features around 14500 Å in kilonova spectra, even considering the uncertainties. This supports the identification of Ce in the observed spectra of AT2017gfo (Domoto et al. 2022).

We have also shown that the F-type supergiants with near solar metallicity show strong absorption of Ce III. To our knowledge, this is the first report of the detection of the Ce III lines at the H-band in stars with near solar abundances. As the line blending is not severe in the NIR spectra compared with the optical spectra, those lines may also be useful for stellar spectroscopic studies.

APPENDIX

A. ABUNDANCE ESTIMATES IN AP STARS AS A TEST OF ASTROPHYSICAL GF-VALUES

We assess the validity of our astrophysical gf-values by adopting them to spectra of Ap stars. Ap stars are a kind of CP stars that exhibit extremely high metal abundances. Thanks to the high abundances, Ap stars show clear Ce III absorption lines that we focus on. However, it is also known that they show inconsistent abundances between singly and doubly ionized rare-earth elements (REE), called REE anomaly (Ryabchikova et al. 2004; Ryabchikova & Romanovskaya 2017). Even if Ce abundances have been measured from Ce II lines, it does not necessarily represent the Ce abundances. Therefore, these stars cannot be used to derive gf-values in Section 4.

Here, we estimate the Ce abundances from Ce III lines (hereafter Ce III abundances) in Ap stars using the derived astrophysical gf-values. We use three Ap stars, HD 101065 (Przybylski's Star), HD 201601 (γ Equ), and HD 24712. These stars have quite different $\log g$ from the supergiants used to derive the gf-values. Thus, the abundance estimates serve as independent assessment of the derived gf-values.

The spectrum of HD 101065 was taken with Gemini south/IGRINS on UT 2022 December 18 in two ABBA sequences with each exposure time of 33 sec. An A0V star (HIP 55019) was also observed for the telluric standard. Those IGRINS spectra are reduced through the pipeline (Lee et al. 2017), as described in Section 3.1. The 1D spectra are normalized by continuum fitting.

The spectra of HD 201601 and HD 24712 were taken with the Gemini Near-Infrared Spectrograph (GNIRS, Elias et al. 2006a,b) at Gemini north telescope on UT 2022 July 17 and August 18, respectively. We use 110.5 l/mm grating and long camera with a 0.1" slit, which gives the spectral resolution of $R \sim 17800$. Central wavelength is set to be 1.6 µm to cover the three Ce III lines. HD 201601 and HD 24712 were observed in one and two ABBA sequence(s) with each exposure time of 60 sec, respectively. For the telluric standards, A0V stars (HD 208108 and HD 15130) were also observed. The GNIRS spectra are reduced using the Gemini IRAF package, and followed standard procedure, which includes flat-fielding, sky subtraction, wavelength calibration based on Ar-Xe lamp spectra, and extraction of 1D spectra. The 1D spectra are normalized by continuum fitting. Telluric absorption in the normalized target spectra is corrected by dividing by the normalized spectra of the A0V stars.

The spectra of three Ap stars around the region of the Ce III lines are show in Figure 7. For those spectra, we measure EWs of the three Ce III lines by Gaussian fitting. Then, we perform spectral synthesis as in Section 4 but by changing the Ce abundance and by using the derived gf-values of the Ce III lines. We use the stellar parameters of the Ap stars derived in literatures using optical spectra as summarized in Table 5. Although there are the atmospheric parameters derived using more sophisticated models that consider stratification of elements for all the samples (Shulyak et al. 2009, 2010, 2013), we adopt those derived using 1D atmospheric models (ATLAS) that we use for spectral synthesis. We measure EWs of the Ce III lines in model spectra by Gaussian fitting and compare with the EWs in the observed spectra. Comparison is repeated by varying Ce abundances until the model EWs match with the EWs in the observed spectra.

We show the results of the Ce III abundances estimated using the three Ce III lines in Table 6. It is seen that the line-by-line variation of the abundances is small in each star. This fact demonstrates that the derived gf-values of the Ce III lines are reasonable.

Table 6 also shows the Ce II and III abundances reported in literatures, which confirms clear REE anomaly. It is worth noting that, although Hubrig et al. (2012) showed that the derived Ce III abundances in HD 201601 deviate about 2 dex depending on the lines, the abundances derived by using the three Ce III lines here are consistent with each other. Also, this is the first measurement of the Ce III abundance for HD 24712.
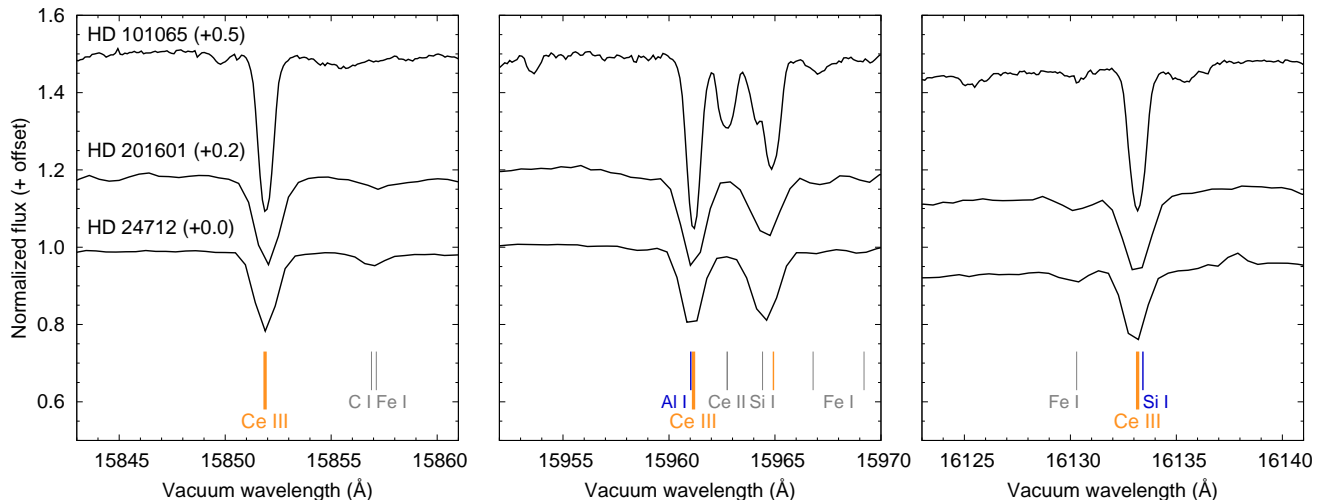

Figure 7. The observed spectra around the Ce III lines of the Ap stars. Absorption lines are labeled as in Figure 1.

REFERENCES

Abbott, B. P., Abbott, R., Abbott, T. D., et al. 2017a,
PhRvL, 119, 161101,
doi: 10.1103/PhysRevLett.119.161101

—. 2017b, ApJL, 848, L12, doi: 10.3847/2041-8213/aa91c9

Table 5. Adopted stellar parameters for the Ap stars.

Star	Model	$T_{\rm eff}$ (K)	$\log g$ (cm s^{-2})	[Fe/H]	ξ (km s^{-1})	$v \sin i$ (km s^{-1})	[Al/H]	[Si/H]	Reference
HD 101065	ATLAS	6600	4.20	−0.72	1.00	3.5	−1.11	0.11	Cowley et al. (2000)
HD 201601	ATLAS	7700	4.20	0.19	2.00	7.0^a	0.66	0.11	Ryabchikova et al. (1997a)
HD 24712	ATLAS	7250	4.20	−0.21	1.00	6.6^a	0.06	−0.18	Ryabchikova et al. (1997b)

Note— All $v \sin i$ are smaller than spectral resolution ($R \sim 45000$ or 17800) and does not affect results.
^{a} Adopted from Sikora et al. (2019).

Table 6. Ce abundances derived using Ce III or II lines in the Ap stars.

[Ce/H]		HD 101065	HD 201601	HD 24712
Ce III	15851.880 Å	4.11	4.09	3.86
	15961.157 Å	4.06	4.04	3.72
	16133.170 Å	4.16	4.26	3.83
	Mean ± standard error	4.11±0.03	4.13±0.07	3.78±0.03
	Literatures	4.76^a	3.46–5.36^c	
Ce II		2.93^a	1.26^d	1.42^e
		3.07^b		

Note— ^{a} Shulyak et al. (2010). ^{b} Cowley et al. (2000). ^{c} Hubrig et al. (2012). ^{d} Ryabchikova et al. (1997a). ^{e} Ryabchikova et al. (1997b).

Abt, H. A., & Morrell, N. I. 1995, ApJS, 99, 135, doi: 10.1086/192182

Adelman, S. J., Snow, T. P., Wood, E. L., et al. 2001, MNRAS, 328, 1144, doi: 10.1046/j.1365-8711.2001.04936.x

Arcavi, I., Hosseinzadeh, G., Howell, D. A., et al. 2017, Nature, 551, 64, doi: 10.1038/nature24291

Asplund, M., Grevesse, N., Sauval, A. J., & Scott, P. 2009, ARA&A, 47, 481, doi: 10.1146/annurev.astro.46.060407.145222

Biémont, E., Palmeri, P., & Quinet, P. 1999, Ap&SS, 269, 635, doi: 10.1023/A:1017049314691

Biémont, E., Quinet, P., & Ryabchikova, T. A. 2002, MNRAS, 336, 1155, doi: 10.1046/j.1365-8711.2002.05868.x

Blanco-Cuaresma, S. 2019, MNRAS, 486, 2075, doi: 10.1093/mnras/stz549

Blanco-Cuaresma, S., Soubiran, C., Heiter, U., & Jofré, P. 2014, A&A, 569, A111, doi: 10.1051/0004-6361/201423945

Carvajal Gallego, H., Palmeri, P., & Quinet, P. 2021, MNRAS, 501, 1440, doi: 10.1093/mnras/staa3729

Castelli, F., & Kurucz, R. L. 1994, A&A, 281, 817

Castelli, F., & Kurucz, R. L. 2003, in Modelling of Stellar Atmospheres, ed. N. Piskunov, W. W. Weiss, & D. F. Gray, Vol. 210, A20, doi: 10.48550/arXiv.astro-ph/0405087

Chojnowski, S. D., Hubrig, S., Hasselquist, S., et al. 2019, ApJL, 873, L5, doi: 10.3847/2041-8213/ab0750

Cowley, C. R., Ryabchikova, T., Kupka, F., et al. 2000, MNRAS, 317, 299, doi: 10.1046/j.1365-8711.2000.03578.x

Cunha, K., Smith, V. V., Hasselquist, S., et al. 2017, ApJ, 844, 145, doi: 10.3847/1538-4357/aa7beb

De Smedt, K., Van Winckel, H., Kamath, D., et al. 2016, A&A, 587, A6, doi: 10.1051/0004-6361/201527430

Domoto, N., Tanaka, M., Kato, D., et al. 2022, ApJ, 939, 8, doi: 10.3847/1538-4357/ac8c36

Domoto, N., Tanaka, M., Wanajo, S., & Kawaguchi, K. 2021, ApJ, 913, 26, doi: 10.3847/1538-4357/abf358

Eichler, D., Livio, M., Piran, T., & Schramm, D. N. 1989, Nature, 340, 126, doi: 10.1038/340126a0

Elias, J. H., Joyce, R. R., Liang, M., et al. 2006a, in Society of Photo-Optical Instrumentation Engineers (SPIE) Conference Series, Vol. 6269, Ground-based and Airborne Instrumentation for Astronomy, ed. I. S. McLean & M. Iye, 62694C, doi: 10.1117/12.671817

Elias, J. H., Rodgers, B., Joyce, R. R., et al. 2006b, in
Society of Photo-Optical Instrumentation Engineers
(SPIE) Conference Series, Vol. 6269, Ground-based and
Airborne Instrumentation for Astronomy, ed. I. S.
McLean & M. Iye, 626914, doi: 10.1117/12.671765

Evans, P. A., Cenko, S. B., Kennea, J. A., et al. 2017,
Science, 358, 1565, doi: 10.1126/science.aap9580

Freiburghaus, C., Rosswog, S., & Thielemann, F. K. 1999,
ApJL, 525, L121, doi: 10.1086/312343

Ghazaryan, S., Alecian, G., & Hakobyan, A. A. 2018,
MNRAS, 480, 2953, doi: 10.1093/mnras/sty1912

Gillanders, J. H., Smartt, S. J., Sim, S. A., Bauswein, A., &
Goriely, S. 2022, MNRAS, 515, 631,
doi: 10.1093/mnras/stac1258

Goriely, S., Bauswein, A., & Janka, H.-T. 2011, ApJL, 738,
L32, doi: 10.1088/2041-8205/738/2/L32

Gray, D. F. 2005, The Observation and Analysis of Stellar
Photospheres (Cambridge University Press),
doi: 10.1017/cbo9781316036570

Gustafsson, B., Edvardsson, B., Eriksson, K., et al. 2008,
A&A, 486, 951, doi: 10.1051/0004-6361:200809724

Hasselquist, S., Shetrone, M., Cunha, K., et al. 2016, ApJ,
833, 81, doi: 10.3847/1538-4357/833/1/81

Hinkel, N. R., Timmes, F. X., Young, P. A., Pagano, M. D.,
& Turnbull, M. C. 2014, AJ, 148, 54,
doi: 10.1088/0004-6256/148/3/54

Hinkel, N. R., Young, P. A., Pagano, M. D., et al. 2016,
ApJS, 226, 4, doi: 10.3847/0067-0049/226/1/4

Holtzman, J. A., Hasselquist, S., Shetrone, M., et al. 2018,
AJ, 156, 125, doi: 10.3847/1538-3881/aad4f9

Hony, S., Tielens, A. G. G. M., Waters, L. B. F. M., & de
Koter, A. 2003, A&A, 402, 211,
doi: 10.1051/0004-6361:20030240

Horne, K. 1986, PASP, 98, 609, doi: 10.1086/131801

Hubrig, S., Castelli, F., González, J. F., et al. 2012, A&A,
542, A31, doi: 10.1051/0004-6361/201218968

Johansson, S., & Litzén, U. 1972, PhyS, 6, 139,
doi: 10.1088/0031-8949/6/2-3/007

Kasen, D., Metzger, B., Barnes, J., Quataert, E., &
Ramirez-Ruiz, E. 2017, Nature, 551, 80,
doi: 10.1038/nature24453

Kawaguchi, K., Shibata, M., & Tanaka, M. 2018, ApJL,
865, L21, doi: 10.3847/2041-8213/aade02

—. 2020, ApJ, 889, 171, doi: 10.3847/1538-4357/ab61f6

Korobkin, O., Rosswog, S., Arcones, A., & Winteler, C.
2012, MNRAS, 426, 1940,
doi: 10.1111/j.1365-2966.2012.21859.x

Kupka, F., Piskunov, N., Ryabchikova, T. A., Stempels,
H. C., & Weiss, W. W. 1999, A&AS, 138, 119,
doi: 10.1051/aas:1999267

Lee, J.-J., Gullikson, K., & Kaplan, K. 2017, Igrins/Plp
2.2.0, Zenodo, Zenodo, doi: 10.5281/zenodo.845059

Li, L.-X., & Paczyński, B. 1998, ApJL, 507, L59,
doi: 10.1086/311680

Luck, R. E. 2014, AJ, 147, 137,
doi: 10.1088/0004-6256/147/6/137

Lyubimkov, L. S., Lambert, D. L., Kaminsky, B. M., et al.
2012, MNRAS, 427, 11,
doi: 10.1111/j.1365-2966.2012.21617.x

Mace, G., Kim, H., Jaffe, D. T., et al. 2016, in Society of
Photo-Optical Instrumentation Engineers (SPIE)
Conference Series, Vol. 9908, Ground-based and Airborne
Instrumentation for Astronomy VI, ed. C. J. Evans,
L. Simard, & H. Takami, 99080C,
doi: 10.1117/12.2232780

Mace, G., Sokal, K., Lee, J.-J., et al. 2018, in Society of
Photo-Optical Instrumentation Engineers (SPIE)
Conference Series, Vol. 10702, Ground-based and
Airborne Instrumentation for Astronomy VII, ed. C. J.
Evans, L. Simard, & H. Takami, 107020Q,
doi: 10.1117/12.2312345

Majewski, S. R., Schiavon, R. P., Frinchaboy, P. M., et al.
2017, AJ, 154, 94, doi: 10.3847/1538-3881/aa784d

Mashonkina, L., Ryabchikova, T., & Ryabtsev, A. 2005,
A&A, 441, 309, doi: 10.1051/0004-6361:20053085

Matsunaga, N., Taniguchi, D., Jian, M., et al. 2020, ApJS,
246, 10, doi: 10.3847/1538-4365/ab5c25

Meléndez, J., & Barbuy, B. 1999, ApJS, 124, 527,
doi: 10.1086/313261

Metzger, B. D., Martínez-Pinedo, G., Darbha, S., et al.
2010, MNRAS, 406, 2650,
doi: 10.1111/j.1365-2966.2010.16864.x

Park, C., Jaffe, D. T., Yuk, I.-S., et al. 2014, in Society of
Photo-Optical Instrumentation Engineers (SPIE)
Conference Series, Vol. 9147, Ground-based and Airborne
Instrumentation for Astronomy V, ed. S. K. Ramsay, I. S.
McLean, & H. Takami, 91471D, doi: 10.1117/12.2056431

Perego, A., Radice, D., & Bernuzzi, S. 2017, ApJL, 850,
L37, doi: 10.3847/2041-8213/aa9ab9

Pian, E., D'Avanzo, P., Benetti, S., et al. 2017, Nature,
551, 67, doi: 10.1038/nature24298

Piskunov, N. E., Kupka, F., Ryabchikova, T. A., Weiss,
W. W., & Jeffery, C. S. 1995, A&AS, 112, 525

Plez, B. 2012, Turbospectrum: Code for spectral synthesis,
Astrophysics Source Code Library, record ascl:1205.004.
http://ascl.net/1205.004

Puķītis, K., Začs, L., & Grankina, A. 2022, ApJ, 928, 29,
doi: 10.3847/1538-4357/ac4bc8

Quinet, P., & Palmeri, P. 2020, Atoms, 8, 18,
doi: 10.3390/atoms8020018

Rosswog, S., Sollerman, J., Feindt, U., et al. 2018, A&A, 615, A132, doi: 10.1051/0004-6361/201732117

Ryabchikova, T., Nesvacil, N., Weiss, W. W., Kochukhov, O., & Stütz, C. 2004, A&A, 423, 705, doi: 10.1051/0004-6361:20041012

Ryabchikova, T., Piskunov, N., Kurucz, R. L., et al. 2015, PhyS, 90, 054005, doi: 10.1088/0031-8949/90/5/054005

Ryabchikova, T. A., Adelman, S. J., Weiss, W. W., & Kuschnig, R. 1997a, A&A, 322, 234

Ryabchikova, T. A., Landstreet, J. D., Gelbmann, M. J., et al. 1997b, A&A, 327, 1137

Ryabchikova, T. A., & Romanovskaya, A. M. 2017, Astronomy Letters, 43, 252, doi: 10.1134/S1063773717040065

Shetrone, M., Bizyaev, D., Lawler, J. E., et al. 2015, ApJS, 221, 24, doi: 10.1088/0067-0049/221/2/24

Shibata, M., Fujibayashi, S., Hotokezaka, K., et al. 2017, PhRvD, 96, 123012, doi: 10.1103/PhysRevD.96.123012

Shulyak, D., Ryabchikova, T., Kildiyarova, R., & Kochukhov, O. 2010, A&A, 520, A88, doi: 10.1051/0004-6361/200913750

Shulyak, D., Ryabchikova, T., & Kochukhov, O. 2013, A&A, 551, A14, doi: 10.1051/0004-6361/201220425

Shulyak, D., Ryabchikova, T., Mashonkina, L., & Kochukhov, O. 2009, A&A, 499, 879, doi: 10.1051/0004-6361/200911623

Sikora, J., Wade, G. A., Power, J., & Neiner, C. 2019, MNRAS, 483, 2300, doi: 10.1093/mnras/sty3105

Smartt, S. J., Chen, T. W., Jerkstrand, A., et al. 2017, Nature, 551, 75, doi: 10.1038/nature24303

Smith, V. V., Bizyaev, D., Cunha, K., et al. 2021, AJ, 161, 254, doi: 10.3847/1538-3881/abefdc

Soubiran, C., Le Campion, J.-F., Brouillet, N., & Chemin, L. 2016, A&A, 591, A118, doi: 10.1051/0004-6361/201628497

Straizys, V., Cernis, K., & Hayes, D. S. 1985, Ap&SS, 112, 251, doi: 10.1007/BF00653507

Tanaka, M., & Hotokezaka, K. 2013, ApJ, 775, 113, doi: 10.1088/0004-637X/775/2/113

Tanaka, M., Hotokezaka, K., Kyutoku, K., et al. 2014, ApJ, 780, 31, doi: 10.1088/0004-637X/780/1/31

Tanaka, M., Kato, D., Gaigalas, G., & Kawaguchi, K. 2020, MNRAS, 496, 1369, doi: 10.1093/mnras/staa1576

Tanaka, M., Utsumi, Y., Mazzali, P. A., et al. 2017, PASJ, 69, 102, doi: 10.1093/pasj/psx121

Tanaka, M., Kato, D., Gaigalas, G., et al. 2018, ApJ, 852, 109, doi: 10.3847/1538-4357/aaa0cb

Tanaka, M., Domoto, N., Aoki, W., et al. 2023, ApJ, 953, 17, doi: 10.3847/1538-4357/acdc95

Tanvir, N. R., Levan, A. J., González-Fernández, C., et al. 2017, ApJL, 848, L27, doi: 10.3847/2041-8213/aa90b6

Tarumi, Y., Hotokezaka, K., Domoto, N., & Tanaka, M. 2023, arXiv e-prints, arXiv:2302.13061, doi: 10.48550/arXiv.2302.13061

Uesugi, A., & Fukuda, I. 1970, Catalogue of rotational velocities of the stars (Faculty of Science, Kyoto University)

Utsumi, Y., Tanaka, M., Tominaga, N., et al. 2017, PASJ, 69, 101, doi: 10.1093/pasj/psx118

Valenti, S., Sand, D. J., Yang, S., et al. 2017, ApJL, 848, L24, doi: 10.3847/2041-8213/aa8edf

Wanajo, S., Sekiguchi, Y., Nishimura, N., et al. 2014, ApJL, 789, L39, doi: 10.1088/2041-8205/789/2/L39

Watson, D., Hansen, C. J., Selsing, J., et al. 2019, Nature, 574, 497, doi: 10.1038/s41586-019-1676-3

Wyart, J.-F., & Palmeri, P. 1998, PhyS, 58, 368, doi: 10.1088/0031-8949/58/4/013